J Mater Sci (2009) 44:5428–5440
DOI 10.1007/s10853-009-3621-6

FERROELECTRICS

Fabrication and characterization of perovskite ferroelectric PMN/PT ceramic nanocomposites

R. Wongmaneerung · R. Yimnirun · S. Ananta

Received: 15 March 2009 / Accepted: 18 May 2009 / Published online: 2 June 2009

Abstract The potential of a ceramic nanocomposite technique employing a simple bimodal particle size packing and a pressureless sintering process as a low-cost and simple ceramic processing to obtain perovskite ferroelectric ceramics in the PMN/PT system was demonstrated. Attention was focused on relationships between chemical composition, densification, microstructure, and electrical properties. It has been found that the phase formation, microstructures, and dielectric properties of ceramic nanocomposites are totally different from those of typical solid solutions.

Introduction

During the past several years, many experimental studies were carried out on various phase transformation and crystal structures of lead-based solid solutions consisting of normal and relaxor perovskite ferroelectrics [1–3]. These compounds have attracted a growing fundamental and practical interest because of their excellent dielectric, piezoelectric, and electrostriction properties which are useful in actuating and sensing applications [4–6]. There is considerable interest in lead magnesium niobate-lead titanate $(1 - x)Pb(Mg_{1/3}Nb_{2/3})O_3$–$xPbTiO_3$, referred to as PMN–PT, ceramics due to their high strains with low hysteresis losses [7–9]. Also, the compound exhibits a broad maximum in the dielectric constant, and the temperature of the dielectric maximum increases with the testing frequency. Moreover, It is an attractive replacement for $BaTiO_3$ in multilayer capacitors (if the X7R temperature characteristics are obtained) because it can be sintered at low temperature in comparison to $BaTiO_3$ [4, 6]. For high performance it is essential that the material be of the perovskite crystalline phase with little or no pyrochlore phase. In the processing of perovskite PMN–PT, the formation of an unwanted pyrochlore phase has long been recognized as a major problem [7–9]. Numerous attempts have been made so far to develop a processing technique in which the formation of undesirable pyrochlore phase is suppressed. Among these, the columbite processing technique [2, 8] has been widely used in the synthesis of phase-pure perovskite PMN-based materials. In this study, an alternative corundum $Mg_4Nb_2O_9$ precursor previously advocated by our group [9, 10] will be used for the preparation of the PMN component.

In addition to the above-mentioned difficulties in the processing of phase-pure PMN–PT solid solutions, another area of concern, which has an important bearing on the dielectric properties of these materials, is the densification behavior and associated microstructure development of the ceramics using various additives that form liquid phase at low temperatures. In most cases, minor additions of excess MgO and/or PbO are used as additives to enhance the densification process, which, in turn, results in an enhancement of the dielectric properties of the sintered materials [8, 11, 12]. However, it should be noted that

R. Wongmaneerung
Department of Physics, Faculty of Science, Maejo University, Chiang Mai 50290, Thailand

R. Yimnirun
School of Physics, Institute of Science, Suranaree University of Technology, Nakhon Ratchasima 30000, Thailand

S. Ananta (✉)
Department of Physics and Materials Science, Faculty of Science, Chiang Mai University, Chiang Mai 50200, Thailand
e-mail: suponananta@yahoo.com

sintering of ceramics to a high density in presence of a liquid phase is not always the objective for obtaining superior dielectric properties of capacitor materials. On the other hand, formation of equilibrium phase assemblages with minor additions of the one or more secondary phases and optimizing the sintering conditions are far more important for the development of a homogeneous microstructure exhibiting the desired grain morphology and grain boundary characteristics with superior dielectric properties.

Ever since the concept of designing ceramics using the "nanocomposites" approach was proposed by Niihara [13] and later modified by Kuntz et al. [14], there has been continued interest in the use of fine particles to improve a variety of properties. Perovskite-based ceramic nanocomposites were found in many previous works [15–18]. Hwang et al. [15] selected MgO and $BaTiO_3$ as a matrix and secondary phase dispersoid and used conventional hot pressing or pulse electric current sintering (PECS) for preparing particle-dispersed ceramic nanocomposites. The $BaTiO_3$ dispersoid in the nanocomposite prepared by the PECS technique showed higher XRD peak splitting than the hot-pressed nanocomposite, indicating better ferroelectricity in the $MgO/BaTiO_3$ nanocomposites. This research group [16] also fabricated PZT/Ag nanocomposites by using conventional powder metallurgical method. It was also found that adding nanosized Ag particles enhanced the mechanical and piezoelectric properties of the PZT ceramics. Tajima et al. [17] reported that the fracture strength and hardness of PZT nanocomposites with 0.5 vol.% Al_2O_3 or 0.1 vol.% MgO additives were significantly improved. From these literatures, it is seen that the intergranular and intragranular types of nanocomposite structure are typically observed in the perovskite ceramic nanocomposites. The remarkable characteristics of these ceramic nanocomposites are summarized as significant or moderate improvement in mechanical properties. However, little attention has been paid directly to the fabrication of the ceramic nanocomposites containing both phases of perovskite ferroelectric nanodispersoid and matrix [18]. Recently, our group [19] has also demonstrated that the microstructures and the dielectric properties of the ceramic nanocomposites are totally different from those of the ceramic solid solutions in the PZT–BT system. A single phase of dense ceramics was found in solid solutions whereas two different phases are visible in the microstructure of the ceramic nanocomposites. The dielectric behavior of the ceramic nanocomposites displayed superposition of two phase transitions, with a lower peak value of the dielectric constant compared with the solid solutions. Based on our previous work [18, 19], the idea of ceramic nanocomposite approach could be applied to other perovskite ferroelectric materials such as PMN–PT. Thus, this study deals with work carried out to fabricate ceramic nanocomposite in the PMN–PT system using the bimodal particle size packing concept. The relationships between processing conditions, microstructures, and electrical properties of PMN–PT ceramic nanocomposites will be established, and compared with those obtained from the conventional solid solution approach. The effect of processing parameters on the arrangement of phases, microstructural evolution, and properties of the ceramics will be carefully investigated.

Experimental procedure

The compositions of the perovskite ferroelectric system $(1 - x)$PMN–xPT ($0.1 \leq x \leq 0.5$) were designed for fabrication of PMN/PT ceramic nanocomposites by using the concept of bimodal particle size (micron-sized PMN + nano-sized PT powders), whereby the dispersed phase of nanosized PT component cannot have a higher concentration than its matrix phase counterpart [17–19]. Between the two end components (i.e., PMN and PT), it was decided to employ PT nanopowders as dispersed phase owing to its easier perovskite formation and higher internal stress [6, 20]. Commercially available powders of PbO, MgO (Fluka, >99% purity), Nb_2O_5, and TiO_2 (Aldrich, >99% purity), with an average particle size of 3 to 5 μm, were used as raw materials. In order to avoid unwanted pyrochlore phases, micron-sized PMN powders were prepared from these oxides using a corundum $Mg_4Nb_2O_9$ *B*-site precursor technique [9, 10]. Nanosized PT powders were also separately synthesized by using vibro-milling technique [21]. The characteristics of each PMN and PT powders and their processing details are described in our previous works [10, 21]. In the mixing process, the calculated relevant proportions of constituents were weighed, suspended in ethanol, and intimately mixed in a vibro-mill without grinding media. Drying was carried out for 2 h (the sample dish was placed on a hotplate with the magnetic stirring in action to prevent gravitational separation of the components) and the dried powder was then ground into the fine powders. Each $(1 - x)$PMN–xPT powder was mixed with approximately 3 wt% PVA binder, pressed at 100 MPa into 15 mm diameter pellets by pseudo-uniaxial pressing, and sintered at a temperature between 1100 °C and 1200 °C for 1 h at a heating rate of 5 °C/min. In order to reduce loss of volatile components, e.g., lead, the samples were surrounded with the atmosphere powder of identical chemical composition [18, 22].

Densities of the sintered products were measured by Archimedes technique. X-ray diffraction (XRD; Siemens-D500 diffractometer) was carried out at room temperature using CuK_α radiation to identify the phase formed. The microstructural development was characterized using a

scanning electron microscopy (SEM; JEOL JSM-840A), equipped with an energy dispersive X-ray (EDX) analyzer. Grain sizes of the sintered ceramics were directly estimated from the SEM micrographs. For the electrical measurements the surfaces of the samples were polished with 3 μm Al_2O_3 powders, cleaned ultrasonically, and dried and electroded by sputtering with gold. To ensure good electrical contact, air dry silver paste was applied over the gold electrode. The dielectric measurements were made using an automated measurement system; i.e., an LCR meter (HP-4824A), a nitrogen-fed furnace (9023 Delta design), and a desktop computer (HP-200 series). Polarization measurements were performed using an RT66A ferroelectric test system (Radiant Technologies) in virtual ground mode. Copper wires were attached to both sides of samples using silver epoxy without clamping sample in order to provide free mechanical boundary condition. During the polarization measurement, an electric field of 10–40 kV/cm based on the coercive fields was applied to a sample immersed in silicone oil to prevent the breakdown of the sample. This system is also capable of simultaneous measurement of strain using an LVDT and lock-in amplifier (SR 830 DSP, Stanford Research).

Results and discussion

The X-ray diffraction patterns obtained from PMN–PT ceramic nanocomposites sintered at 1100 and 1200 °C are displayed in Fig. 1a and b, respectively, where the pure

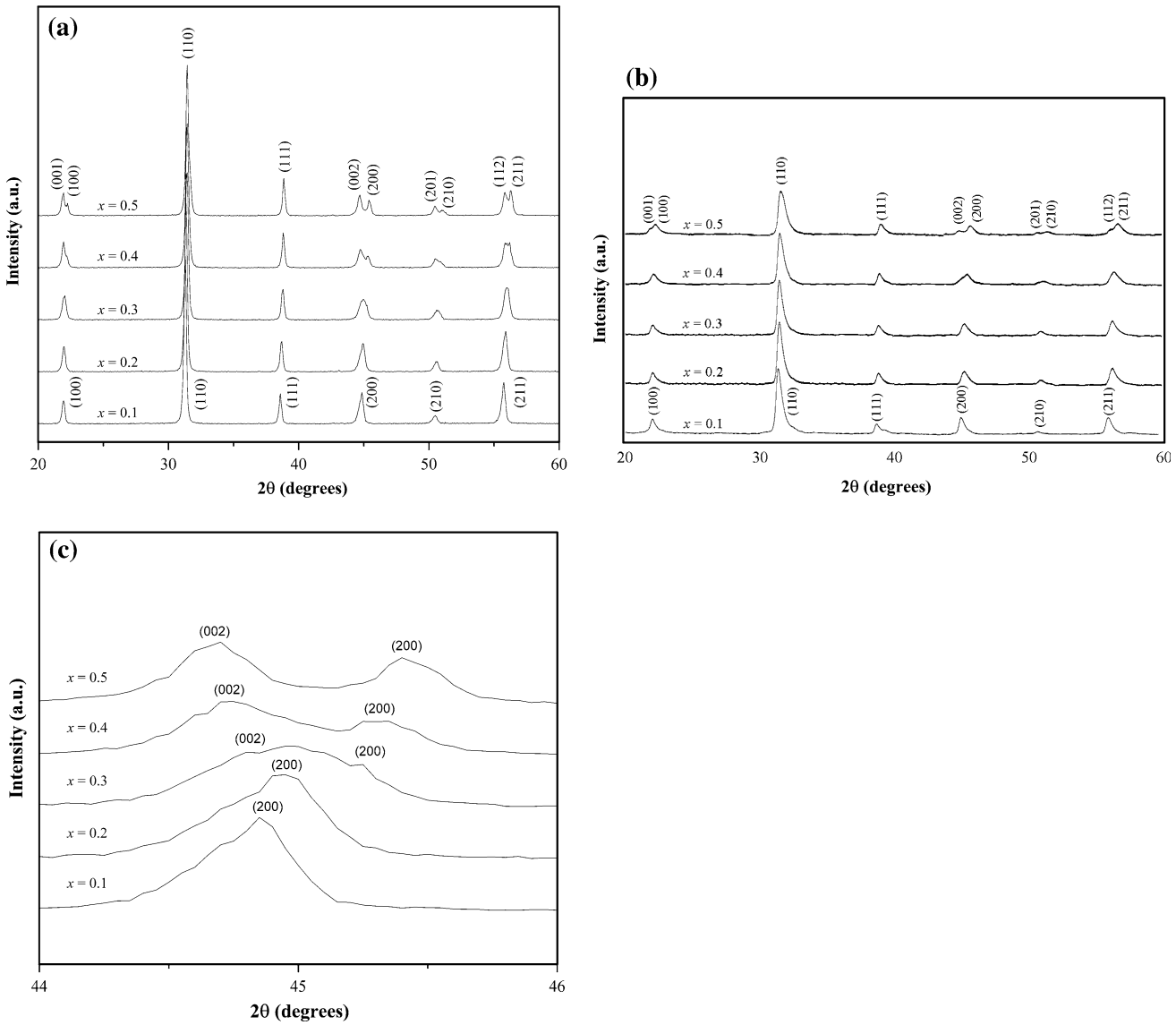

Fig. 1 XRD patterns of (1 − *x*)PMN–*x*PT ceramic nanocomposites sintered at **a** 1100 °C, **b** 1200 °C and **c** enlarged **b**, showing doublets (002) and (200)

perovskite structure was formed throughout the whole composition ranges. In general, it is seen that the XRD peaks of PMN–PT ceramic nanocomposites are broader than those of solid solution [7, 8, 23], consistent with observations made in other similar perovskite ferroelectric systems [19, 20]. These can be interpreted in terms of co-existing perovskite phases, i.e., PMN, PT, and their related intermediate phases. Moreover, a careful observation showed only a pseudo-cubic symmetry at low values of PT concentration, in agreement with other researchers [23, 24]. By the influence of PT, however, several peaks split for $x \geq 0.3$, indicating the development of tetragonal symmetry, which continued with a further increase in PT concentration. For example, (002)/(200) peaks splitting the diffraction line around 2θ of 44–46° are shown in Fig. 1c confirming their tetragonal symmetry, in good agreement with other similar perovskite systems [25, 26]. In general, the strongest reflections in the majority of XRD traces indicate the formation of the perovskite phase which could be matched with a mixture of PMN and PT phases, in agreement with other works [9, 20, 23]. In order to evaluate the relative amounts of perovskite and pyrochlore phases in each composition, the following approximation was used, as in our earlier works [10, 27]:

$$\text{Perovskite phase (wt\%)} = I_p/(I_p + I_m) \times 100 \quad (1)$$

Here I_p and I_m refer to the intensities of the (110) perovskite and (222) minor phase peaks, respectively, these being the most intense reflections in the XRD patterns of both phases. For the purposes of estimating the concentration of minor phase present, Eq. 1 has been applied to the diffraction patterns obtained (Table 1). Within the limitation of the XRD technique in this study, it should be noted that a single phase of perovskite is found in all PMN–PT ceramic nanocomposites, in contrast to the results obtained from the solid solution case [7, 8, 28] (Table 1). No trace of unreacted starting materials or pyrochlore-type phase of Pb–Nb–O compounds reported earlier by other researchers [8, 10, 23] was observed, nor was there any evidence of other second phases [28–30] being present. This could be due to the lower optimized sintering temperature of the nanocomposites as compared to the solid solution, leading to a smaller degree of PbO volatilization and consequently avoiding the unwanted phase formation, consistent with literature [30–32], while a sufficient arrangement of grain-packing required for ceramic densification still was reached. However, many other factors come into play, e.g., homogeneity of materials, reactivity of starting powders, and processing variables. These XRD results clearly show that, in general, the different processing methods used for preparing PMN–PT ceramic nanocomposites gave rise to a different phase

Table 1 Physical properties of $(1 - x)$PMN–xPT ceramic nanocomposites

Sintering temperature (°C)	Composition (x)	Physical properties		
		Perovskite phase[a] (%)	Density[b] (g/cm^3)	Grain size[c] (μm)
1100 (Nanocomposites)	0.1	100	4.74	0.09–1.95
	0.2	100	5.92	0.18–1.94
	0.3	100	6.59	0.08–1.54
	0.4	100	7.03	0.10–2.73
	0.5	100	7.28	0.09–3.00
1200 (Nanocomposites)	0.1	100	7.06	0.53–3.67
	0.2	100	7.10	0.33–3.34
	0.3	100	7.20	0.52–3.53
	0.4	100	7.23	0.41–4.02
	0.5	100	7.40	0.67–3.13
1220 (Solid solution) [35]	0.1	–	–	–
	0.2	–	–	–
	0.3	–	–	–
	0.4	98.70	7.80	0.42–3.66
	0.5	100	7.77	0.44–3.02
1240 (Solid solution) [35]	0.1	97.22	7.89	0.41–2.80
	0.2	100	7.94	0.41–3.45
	0.3	100	7.86	0.48–3.72
	0.4	–	–	–
	0.5	–	–	–

[a] The estimated precision of the phase concentration is ±0.1%

[b] The estimated precision of the density is ±0.05 g/cm^3

[c] The estimated precision of the grain size is ±0.05 μm

formation in the sintered materials. The absence of minor phase in composite samples was related to the more reactive process used.

The representative XRD patterns of 0.5PMN–0.5PT ceramic nanocomposites as a function of sintering temperature, together with that from a true solid solution, are shown in Fig. 2a. As expected, distinct peaks from the two perovskite phases are visible at low sintering temperature of 900 °C. As the sintering temperature increased to 1100 °C, the two phases begin to coalesce and form a nanocomposite microstructure with very narrow peak width. Further increase in the sintering temperature to 1200 °C results in a peak width broadening, similar to that of the true solid solution as plotted on the top. For better quantitative comparison, the full-width at half maximum of (100), (110), and (111) peaks is also plotted as a function of sintering temperature in Fig. 2b. One can easily see that a very narrow peak width is observed at the sintering temperature of 1100 °C where a nanocomposite microstructure exists, while a broader peak width is displayed at lower sintering temperature where the two phases coexist and at high sintering temperature where the true solid solution forms. Further TEM study should clearly distinguish the relaxor-like structure of the PMN from the tetragonal domain structure of the PT phase. However, this aspect is beyond the scope the present paper.

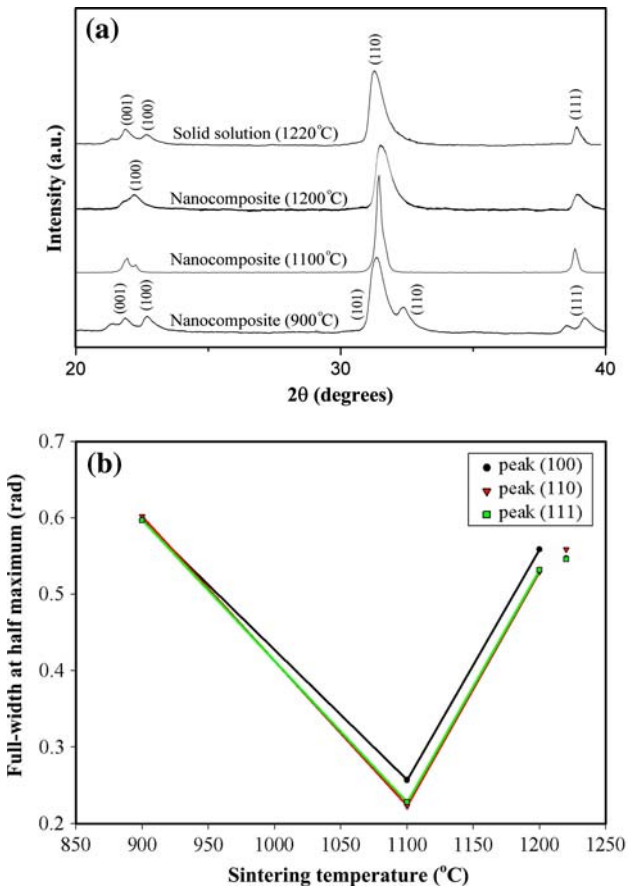

Fig. 2 **a** XRD patterns and **b** full-width at half maximum of the XRD peaks as a function of sintering temperature for 0.5PMN–0.5PT ceramic nanocomposites, compared with a true solid solution sintered at 1220 °C

The densification and grain size data of all PMN–PT ceramic nanocomposites are compared with those of the solid solutions available in the literature, as given in Table 1. In general, the bulk density was found to increase with firing temperature and PT content, which could be due to the lower melting point of PT compared to PMN [4, 9, 29]. Thus, the admixture of PMN could be considered to be a useful technique for promoting the densification of PT, along with its other significant advantage of bringing the Curie range down to lower temperatures as demonstrated (Figs. 6 and 7) by a number of researchers [9, 33, 34]. It is also interesting to note that in this study the effects of both sintering temperature and the amount of PT nanoparticles were found to be significant for the densification of PMN–PT ceramic nanocomposites. Density values of about 4.74–7.28 and 7.06–7.40 g/cm^3 were obtained after sintering at 1100 and 1200 °C, respectively, which are considerably lower than the values obtained for sintered PMN–PT solid solution ceramics [35] (Table 1). Different optimized firing temperatures used may be responsible for these different final densification results. It can be seen that for a given chemical composition, the density values of ceramics sintered at 1100 °C are lower than the values of ceramics sintered at 1200 °C, especially for the case of low PT concentration. In order to preserve the ceramics with nanostructural arrangement, it is possible that the employed sintering temperature in this work is not enough for driving densification mechanism to achieve fully dense PMN–PT ceramic nanocomposites. However, so far, there are no reports on the production of highly dense PMN–PT ceramic nanocomposites by a pressureless sintering method. Moreover, the scope of improving pressureless sintering by raising the temperature is limited by the melting point of both PMN and PT end components (~1300 °C) while the hot-pressing method can cause severe problems related to the evaporation of PbO [36]. Furthermore, in Table 1, it can be seen that grain sizes of ceramic nanocomposites sintered at lower temperature are smaller than those obtained in ceramics sintered at higher temperature, especially for the compositions with high PT content. Besides the effect of sintering temperature, another possible reason is that the incorporation of second phase (as later confirmed by SEM technique) could limit grain growth in the matrix.

The key mechanisms responsible for the lower sintering temperature observed in this work are still unclear. The higher green densities may be attributed to the employed bimodal particle size method via both geometric interlocking and improved cohesion between particles.

Interlocking is the primary strengthening mechanism for irregular shaped particles, especially for low compaction pressure [37] where pressureless sintering was used. However, other possibilities such as starting powder characteristics, the behavior of powder agglomerates with a single pressing operation during powder compaction, the pressure gradient that exists in the larger particles, and heating/cooling rates may also share their responsibility for the final densification of these products.

It should be noted that previously an experiment on the conventional route with bimodal particle distribution technique was carried out and the complete solid solution microstructure type commonly found in the conventional PMN–PT processing was observed at slightly lower sintering temperatures, indicating the solubility effect of the lead-based complex perovskite PMN–PT (although their particle size fractions are different, similar constituent species can have faster interdiffusion rate during firing), and hence limiting the possibility of composite formation [18, 35].

SEM micrographs of $(1 - x)$PMN–xPT ceramic nanocomposites ($x = 0.1$, 0.3, and 0.5) sintered at different temperatures are compared in Fig. 3. In general, the samples show nearly 100% intergranular fracture behavior. With increasing PT content, the grain boundary changed from intergranular to transgranular surface (Fig. 3c). It can also be seen that the specimens only show a few small pores at grain boundaries and triple points; cracks or microcracks were not detected. Moreover, the degree of grain close-packing microstructures tends to increase with PT content. High porosity and heterogeneous microstructures consisting mainly of two ranges of particles (in respect of size and shape) were found in the samples sintered at lower temperature (Fig. 3a–c). A distribution of very small particles with diameter ~100–200 nm is found over the PMN grains. Large pore sizes of the order of 1 μm were also observed. These poorly sintered samples could be attributed to several factors, including the effect of different size fractions between the two different end components,

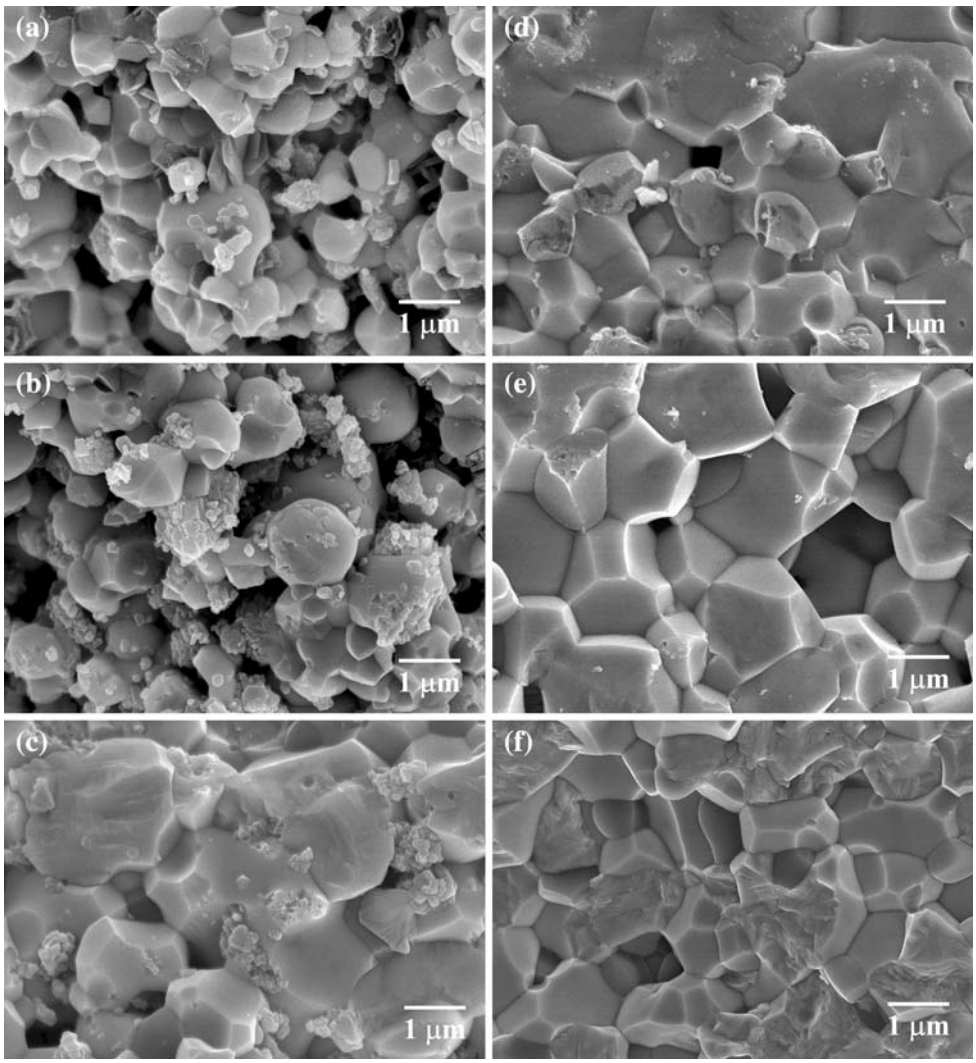

Fig. 3 SEM micrographs of $(1 - x)$PMN–xPT ceramic nanocomposites sintered at 1100 °C with $x =$ **a** 0.1, **b** 0.3 and **c** 0.5; and at 1200 °C with $x =$ **d** 0.1, **e** 0.3 and **f** 0.5

ineffective mixing, and the use of shortened sintering time or low firing temperature, similar to those observed by other researchers [19, 26, 38]. With comparison to the samples sintered at higher temperatures (Fig. 3d–f), different microstructural characteristics are clearly observed.

It should be noted that the overall microstructures of PMN–PT ceramics nanocomposites sintered at 1100 °C are totally different from those observed in the solid solution case [9, 39], although the grain size range between the two systems are about the same (Table 1). On the other hand, the samples sintered at 1200 °C show similar microstructure as the solid solution samples. All samples exhibit uniformly sized grains with a high degree of grain close-packing. Here, the employed sintering temperature is probably high enough for driving diffusion mechanism to achieve the final sintered samples as obtained by the solid-state sintering in the PMN–PT solid solution. Clearly, the ceramic fabrication technique has been found to have a pronounced effect on the phase formation, densification, and microstructure of ceramics in the PMN–PT system [7, 9, 39]. As shown in Fig. 3, two different phases appear in the microstructure, i.e., PMN grains and intergranularly located PT nanoparticles. This kind of microstructure can be matched with the "inter-intragranular" structural model of ceramic nanocomposites proposed by Niihara [13]. Thus, one of the main objectives regarding the fabrication of PMN–PT ceramic nanocomposites by using the bimodal particle size packing concept (micron-sized PMN + nano-sized PT powders) is successfully achieved. This type of ceramic nanocomposite is expected to exhibit good resistance to high temperature creep via the intergranular structure due to grain boundary pinning. Correspondingly, the intragranular configuration hinders crack motion through the grain, i.e., transgranular fracture, and potentially the strength and toughness can be enhanced [14]. However, the rationalization of the various mixed-phase sintering phenomena relies on both physical and chemical factors. The physical factors involve the green powder structure, particle size, particle shape, composition, homogeneity, and green density [18, 37]. For example, a mixture will exhibit a high packing density when there is a large size difference between the particles. In turn, sintering shrinkage depends not only on temperature and time, but also on composition, particle size, phase connectivity, and green density. Hence, mixed particles exhibit widely varying responses to sintering cycles depending on geometric attributes. It can be seen that so many unanswered questions still remain, especially in connection with their electrical properties. These aspects are verified in the following.

The dielectric properties, e.g., dielectric constant (ε_r) and dielectric loss tangent ($\tan\delta$), are measured as functions of both temperature and frequency, as shown in Figs. 4a and 5a for 0.9PMN–0.1PT compositions sintered at 1100 °C and 1200 °C, respectively. As listed in Table 2, the Curie temperature (T_C) (determined at measuring frequency of 1 kHz) increases from 33 (39) °C in 0.9PMN–0.1PT to 270 (268) °C in 0.5PMN–0.5PT sintered at 1100 (1200) °C. This is a direct result of PT addition to PMN ($T_C \sim -8$ °C) since PT itself has a Curie temperature of 490 °C [4, 6]. The Curie temperatures are about the same for each composition measured while their slight variation seems to be related to the effect of firing temperature on density of the final products. As shown in Fig. 4a, for 0.9PMN–0.1PT ceramic nanocomposite sintered at 1100 °C, both ε_r and $\tan\delta$ exhibit strong temperature–frequency dependence below the transition temperature. This is a typical behavior of relaxor ferroelectrics [4, 40], in which strong temperature–frequency dependence is observed, and the temperatures of maximum dielectric constant and dielectric loss tangent are shifted to higher temperature with increasing frequency. The maximum value of the dielectric constant decreases with increasing frequency, while that of the dielectric loss tangent increases. The dielectric properties then become frequency independent above the transition temperature. PMN is a well-known relaxor ferroelectric material as a result of a short-range ordered structure with a nanometer scale heterogeneity in composition [6, 40]. Small addition of PT to PMN causes an increase in T_C, but the strong relaxor behavior still exists. In addition, since 0.9PMN–0.1PT ceramic has a pseudo-cubic symmetry it is intrinsically electrostrictive (i.e., its electrically induced strain is quadratically proportional to the applied electric field and is non-hysteretic, as shown later in Fig. 10) [41, 42]. With its enhanced dielectric properties at room temperature, as listed in Table 2, it is widely employed in transducers and actuators [4–6].

Further increase in PT contents leads to more observable normal ferroelectric behavior because PT is intrinsically a normal ferroelectric [4, 6]. For instance, the dielectric properties of 0.7PMN–0.3PT ceramics sintered at 1200 °C (as plotted in Fig. 5b) exhibit a mixture of both normal and relaxor characteristics, in which the transition temperature is not shifted as much as for relaxor 0.9PMN–0.1PT ceramics. Similar tendency has also been observed in several prior investigations [41–44]. It should be noted that 0.7PMN–0.3PT ceramic composition is close to MPB of the PMN–PT system. Therefore, its structural symmetry is a mixture of pseudo-cubic and tetragonal, which in turn causes a mixture of normal and relaxor characteristics observed for dielectric properties. On the other hand, with a tetragonal symmetry, the 0.5PMN–0.5PT ceramics sintered at 1200 °C exhibit a normal ferroelectric behavior (Fig. 5c), in which the dielectric properties change significantly with temperature, but are nearly independent of frequency, except in the vicinity of the phase transformation temperature. This is a

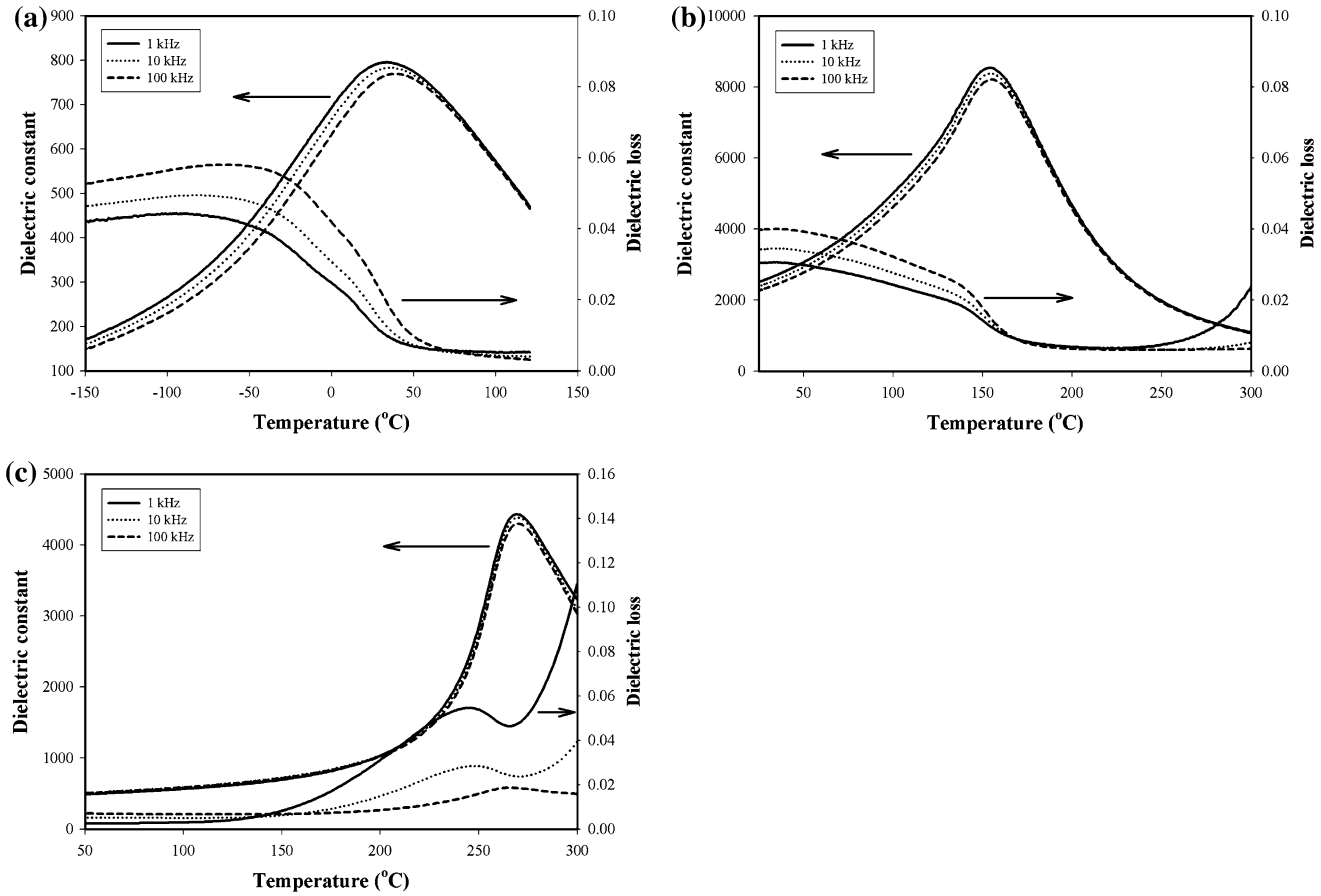

Fig. 4 Variation with temperature and frequency of dielectric properties of $(1 - x)$PMN–xPT ceramic nanocomposites sintered at 1100 °C with $x =$ **a** 0.1, **b** 0.3, and **c** 0.5

typical characteristic of normal ferroelectric ceramics with a long-range ordered structure [40, 45]. It should also be noted here that the dielectric properties in all ceramics increase significantly at high temperature as a result of thermally activated space charge conduction [26, 44].

The temperature dependence of the dielectric properties at 1 kHz of all compositions sintered at 1100 °C and 1200 °C is compared in Figs. 6 and 7, respectively, and the details are given in Table 2. It can be concluded that when PT is added to form the binary system with PMN, the T_C increases monotonically, as shown in Table 2 and Figs. 6 and 7, and the dielectric behavior is shifted from relaxor ferroelectric toward normal ferroelectric. However, the dielectric constant of ceramic nanocomposites samples sintered at 1100 °C is lower than the values of PMN–PT ceramic nanocomposites sintered at 1200 °C (as shown in Table 2) and solid solution ceramics for all compositions. There are various reasons to explain the dielectric response of composite materials. Ausloo [46] studied the effective dielectric constant theories of composite solids. His work reported the broad curve of dielectric constant of the results of clustering effect including the shape of the cluster and particle heterogeneity effect. In this work, it is possible that PT nanoparticles in the samples may hinder domain wall motion and lead to reduced dielectric constant. Another possible reason should be the low density values.

To further understand the dielectric behavior of the PMN–PT ceramic nanocomposites, the ferroelectric transition can analyzed through the Curie–Weiss relationship. For a normal ferroelectric such as PT, above the Curie temperature, the dielectric constant follows the Curie–Weiss law:

$$\varepsilon = c/(T - T_0) \tag{2}$$

where c is the Curie constant and T_0 is the Curie–Weiss temperature [3–6]. For a ferroelectric with a diffuse phase transition such as PMN and PMN–PT compounds, the following equation applies:

$$1/\varepsilon \approx (T - T_m)^2 \tag{3}$$

The above equation has been shown to be valid over a wide temperature range compared with the normal Curie–

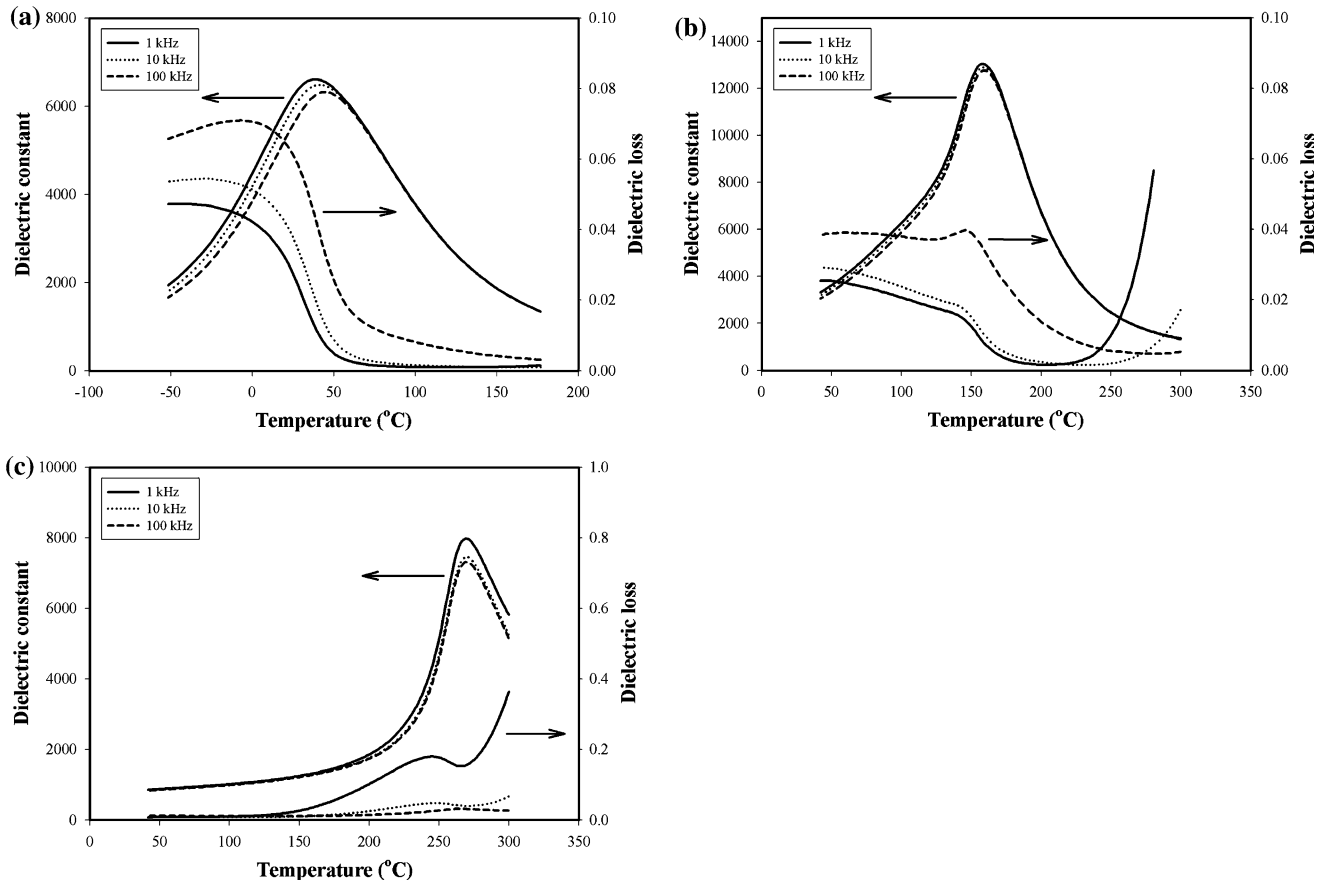

Fig. 5 Variation with temperature and frequency of dielectric properties of $(1 - x)$PMN–xPT ceramic nanocomposites sintered at 1200 °C with x = **a** 0.1, **b** 0.3, and **c** 0.5

Weiss law, Eq. 2 [26, 40]. In Eq. 3, T_m is the temperature at which the dielectric constant is maximum. If the local Curie temperature distribution is Gaussian, the reciprocal permittivity can be written in the form: [3, 26]

$$1/\varepsilon = 1/\varepsilon_m + (T - T_m)^{\gamma}/2\varepsilon_m\delta^2 \quad (4)$$

where ε_m is the maximum permittivity, γ is the diffusivity, and δ is the diffuseness parameter. For $(1 - x)$PMN–xPT compositions, the diffusivity and diffuseness parameters can be estimated from the slope and intercept of the dielectric data displayed in Fig. 8 and Table 2, which should be linear. The values of γ and δ are both material constants depending on the composition and structure of the materials [25, 26]. The value of γ is the expression of the degree of dielectric relaxation, while the parameter δ is used to measure the degree of diffuseness of the phase transition. In a material with the "pure" diffuse phase transition described by the Smolenskii–Isutov relation, Eq. 2, the value of γ is expected to be 2 [40]. The mean value of the diffusivity (γ) is extracted from these plots by fitting a linear equation. The values of γ given in Table 2 vary between 1.53 and 1.97, which confirms that diffuse phase transition occurs in these PMN–PT ceramic nanocomposites. However, the phase transition in this system can be considered as "not purely" diffuse as the γ value is not equal to 2 [40]. It is important to note that in perovskite ferroelectrics, it has been established that γ and δ can be affected by microstructure features, density, and grain size [43, 44]. For PMN–PT ceramic nanocomposites, γ and δ increase with an increase in PMN content, confirming the diffuse phase transitions in PMN–PT ceramic nanocomposites. It is clear that the addition of PT nanoparticles decrease the degree of disorder in $(1 - x)$PMN–xPT over the compositional range $0.1 \leq x \leq 0.5$ with the highest degree of diffuseness exhibited in the 0.9PMN–0.1PT ceramic nanocomposites. It should also be mentioned here that different dielectric behaviors could also be caused by grain size variation and microstructural arrangement (verified by SEM technique in Fig. 3). The microstructural heterogeneity also gives rise to random fields, which tend to make the phase transition "diffuse" instead of sharp as in normal ferroelectric [41–43].

Table 2 Dielectric properties of $(1 - x)$PMN–xPT ceramic nanocomposites

Sintering temperature (°C)	Composition (x)	Dielectric properties (at 1 kHz)					
		T_C (°C)	$\varepsilon_{r,25\ C}$	$\varepsilon_{r,max}$	$\tan\delta_{max}$	γ	δ
1100 (Nanocomposites)	0.1	33	788	794	0.04	1.90	65.79
	0.2	98	2630	5663	0.02	1.72	22.27
	0.3	154	2514	8539	0.02	1.70	3.87
	0.4	213	1743	9722	0.02	1.56	2.91
	0.5	270	475	4433	0.05	1.53	2.28
1200 (Nanocomposites)	0.1	39	6224	6613	0.04	1.92	38.22
	0.2	97	3527	12000	0.03	1.87	26.80
	0.3	158	2807	13048	0.01	1.85	19.85
	0.4	216	1640	9801	0.01	1.80	15.46
	0.5	268	820	7980	0.2	1.75	14.06
1220 (Solid solution) [35]	0.1	–	–	–	–	–	–
	0.2	–	–	–	–	–	–
	0.3	–	–	–	–	–	–
	0.4	220	–	2134	0.02	–	–
	0.5	250	–	1010	0.03	–	–
1240 (Solid solution) [35]	0.1	38	–	19400	0.09	–	–
	0.2	140	–	3520	0.04	–	–
	0.3	197	–	2320	0.02	–	–
	0.4	–	–	–	–	–	–
	0.5	–	–	–	–	–	–

A series of polarization–field (P–E) hysteresis loops for the PMN–PT ceramic nanocomposites sintered at 1200 °C are given in Fig. 9. It is clearly evident that the shape of P–E loops varies greatly with the ceramic compositions. With large amount of normal ferroelectric PT contents, the polarization loops of 0.5PMN–0.5PT and 0.6PMN–0.4PT are well developed showing large remnant polarization (P_r: remaining polarization when electric field is decreased to zero). The hysteresis loops are of a typical "square" form as a result of domain switching in an applied field. This is a typical characteristic of a phase that contains long-range interaction between dipoles in the ferroelectric micro-domain state [40, 45]. This confirms that these compositions are of a normal ferroelectric phase with tetragonal symmetry, as indicated by the dielectric measurements and XRD analysis. The 0.7PMN–0.3PT ceramic shows the largest polarization values with small coercive field (E_C), confirming that the composition is near the MPB of PMN–PT system. The other compositions with more PMN content show more of "slim" hysteresis loops, a characteristic of the suppressed ferroelectric interaction [41, 42, 47]. This is typically found in the relaxor ferroelectrics with polar nano-regions. This has also resulted in the decrease of the values of both P_r and E_C, as seen in Table 3, due to increased pseudo-cubic non-ferroelectric phase content [42–44]. From the loops, the polarizations (P_r and P_s) and the coercive field E_C (indicating an electric field required to zero the polarization) are extracted as given in Table 3. The results clearly suggest that an addition of PT nanoparticles induces the normal ferroelectric behaviors of PT into the PMN–PT ceramic nanocomposites. Moreover, it should be noted that a conclusion drawn from the XRD and dielectric properties measurements discussed earlier that the MPB composition should exist at $x \sim 0.3$ is supported further by the ferroelectric properties, as seen from a strong reduction of polarization values with increasing PT content up to $x = 0.3$, and then a sudden enhancement of the polarization values with further increase in PT content, consistent with those found for the PZT–PCN system [48].

A similar behavior is also observed from the strain–electric field (s–E) relation, as plotted in Fig. 10. As can be seen, the near hysteresis-free electrostrictive behavior normally observed in relaxor ferroelectric is obtained in 0.9PMN–0.1PT ceramic. With increasing amount of PT, the s–E loops become more of "butterfly" type typically obtained in normal ferroelectric state [4–6]. The field-induced strain increases with increasing amount of PT to 30 mol% (near MPB composition), reaching the maximum value of $\sim$0.12%. Further increase in the PT content results in the decrease of the induced strain. Therefore, it can be concluded that the ferroelectric properties of the

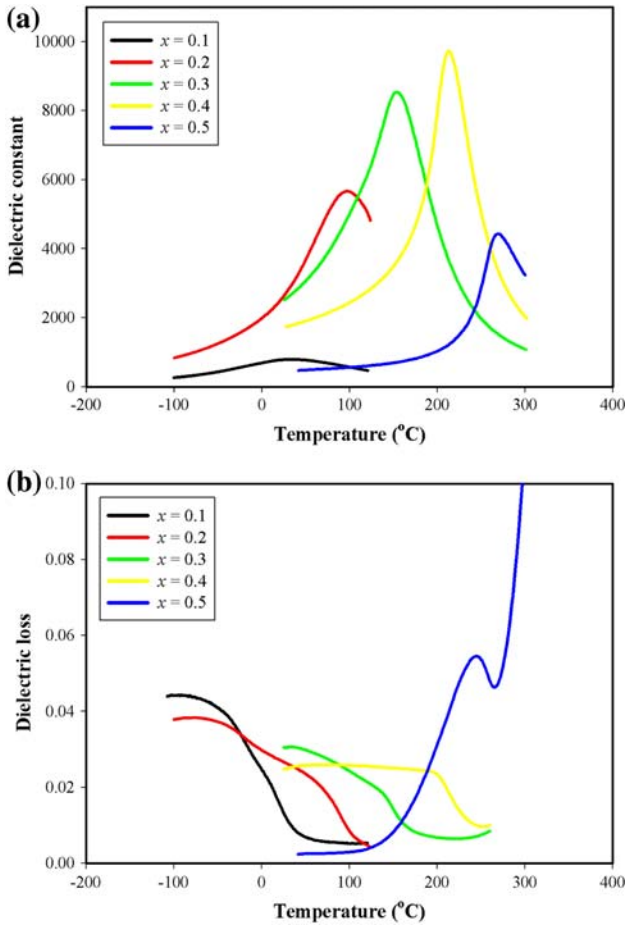

Fig. 6 Variation with temperature of dielectric constant (ε_r) at 1 kHZ for $(1 - x)$PMN–xPT ceramic nanocomposites sintered at 1100 °C

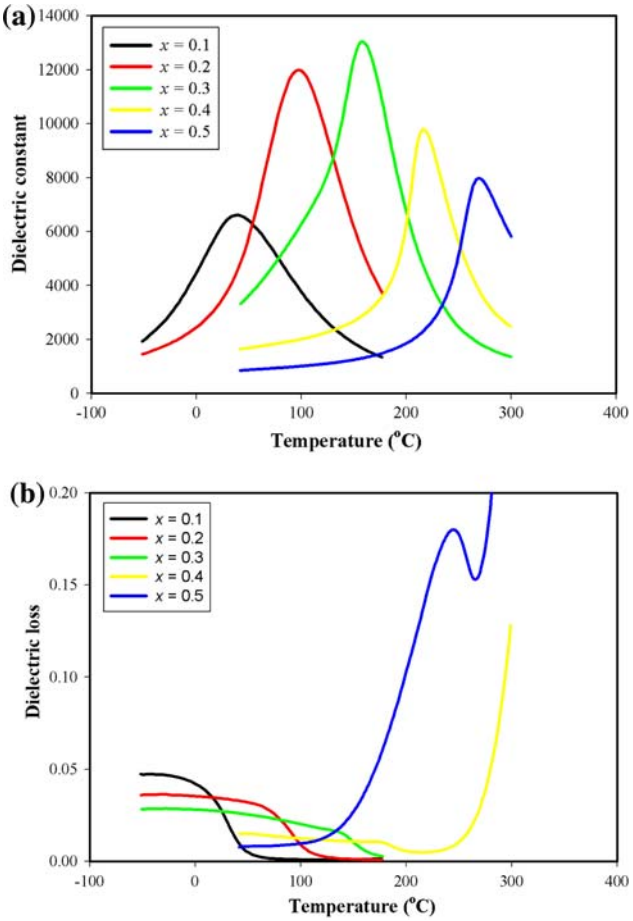

Fig. 7 Variation with temperature of dielectric constant (ε_r) at 1 kHZ for $(1 - x)$PMN–xPT ceramic nanocomposites sintered at 1200 °C

ceramic nanocomposites in PMN–PT system move gradually from the relaxor ferroelectric state in PMN to the normal ferroelectric state in 0.5PMN–0.5PT, crossing the MPB near 0.7PMN–0.3PT [35, 41, 42].

From the dielectric and ferroelectric data, the results and behavior are similar to $(1 - x)$PMN–xPT solid solutions [24, 34, 35]. However, the values of ceramic nanocomposites are slightly lower than those of solid solution ceramics. It is possible that this lower electrical data is due to the reduced domain switching caused by the second phase particles which are incorporated within the matrix grains. Moreover, the dielectric behaviors still exhibit a board peak in all composition. This behavior is different from the solid solution ceramics (showing sharp peak with PT content increasing). It is believed that two dielectric behaviors (relaxor ferroelectric and normal ferroelectric) co-exist in these samples [25, 48].

It should be noted here that the most interesting sample in this study, the sample sintered at 1100 °C, is of relatively low density. Hence, as a result of their lossy characteristics, it is unfortunate that it is not possible to include

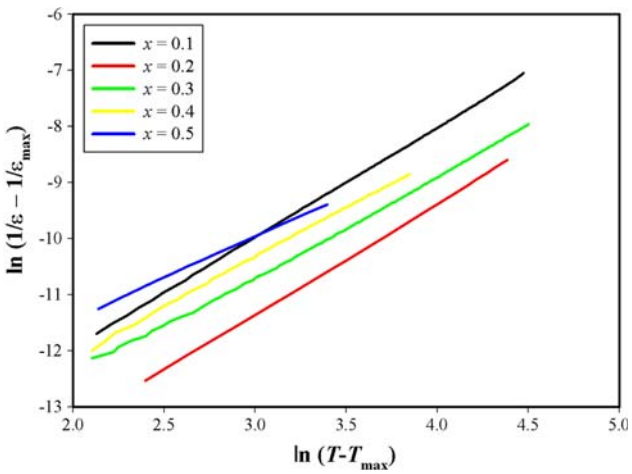

Fig. 8 Variation of $\ln(1/\varepsilon_r - 1/\varepsilon_{max})$ vs $\ln(T - T_{max})$ of $(1 - x)$ PMN–xPT ceramic nanocomposites sintered at 1200 °C

hysteresis or strain data of these compositions that would allow even more interesting comparison between a nanocomposite microstructure and a conventional solid

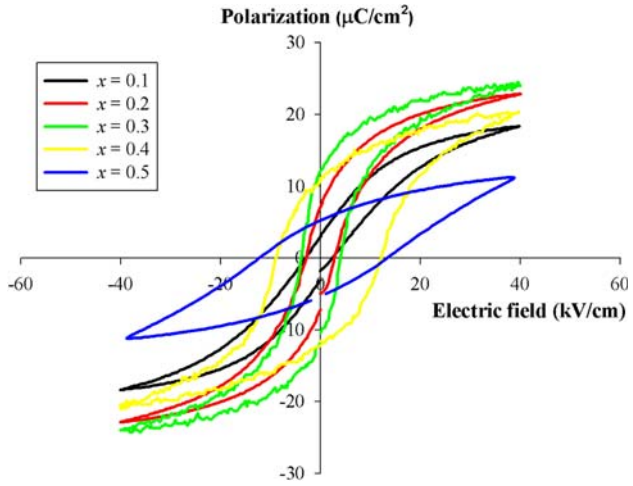

Fig. 9 $P-E$ hysteresis loops of $(1-x)$PMN–xPT ceramic nanocomposites sintered at 1200 °C

solution. If available, one may consider applying the sintering forging method utilized by Frey et al. [49] to obtain a true nanocomposite structure without scarifying density.

The results obtained in this work suggest that, in general, the PMN–PT ceramic nanocomposites exhibit complex microstructures which are inherently heterogeneous. The heterogeneity is a result of variation in grain size and orientation, variation in chemical homogeneity, and the presence and distribution of additional minor phase, pores, and cracks [50, 51]. These factors, which are strongly influenced by the sintering conditions, have an important effect on the dielectric properties of the materials and their reproducibility. Two aspects of this study are significant: (i) reductions in the maximum required sintering temperature (or the required prolong firing time) are possible as compared to the conventional method and (ii) a framework has been established for developing ceramic nanocomposite technique for tailoring new electrical properties of ferroelectric ceramics, particularly those containing low melting point constituents. For better understanding and verifying the attractiveness of the nanocomposite technique further, a systematic study on the effect of other ferroelectric nanodispersoids such as $BaTiO_3$, PNN, or PFW on the phase formation, densification, microstructure, and electrical properties of the ferroelectric-based ceramic nanocomposites is clearly required.

Conclusions

The methodology demonstrated in this study provides a simple method for fabrication of the perovskite ferroelectric PMN–PT ceramic nanocomposites by employing a bimodal particle size packing concept. Their dielectric properties are strongly influenced by the ceramic processing that affects chemical compositions, densification, and microstructure. Under suitable processing conditions, the perovskite phase formation, dielectric constant peak broadening, and dielectric loss of the PMN/PT nanocomposites are better than those obtained from the conventional solid solution approach. Finally, it should be emphasized that this work presents for the first time the effects of

Table 3 Ferroelectric properties of $(1-x)$PMN–xPT ceramic nanocomposites

Sintering temperature (°C)	Composition (x)	Ferroelectric properties (at 25 °C, 0.1 Hz)		
		P_s (μC/cm^2)	P_r (μC/cm^2)	E_C (kV/cm)
1200 (Nanocomposites)	0.1	18.37	3.05	2.37
	0.2	22.84	7.29	2.77
	0.3	25.46	12.14	3.67
	0.4	20.56	11.16	12.19
	0.5	11.25	5.60	13.57
1220 (Solid solution) [35]	0.1	–	–	–
	0.2	–	–	–
	0.3	–	–	–
	0.4	12.75	8.4	8.91
	0.5	7.5	5.3	12.79
1240 (Solid solution) [35]	0.1	10.0	1.3	1.96
	0.2	16.0	5.5	2.36
	0.3	17.9	10.0	8.91
	0.4	–	–	–
	0.5	–	–	–

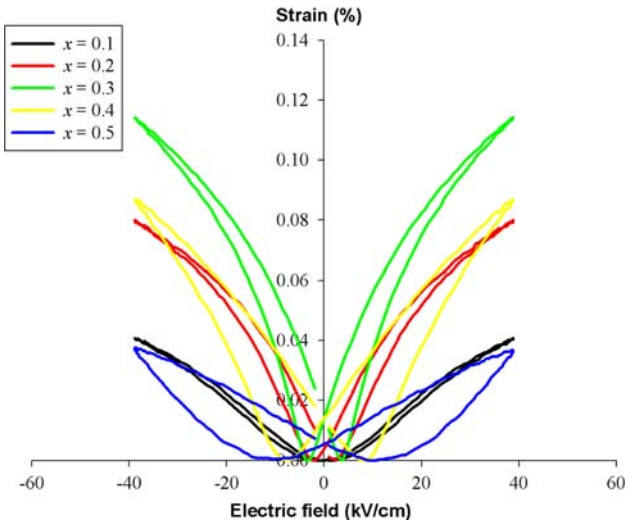

Fig. 10 $s-E$ hysteresis loops of $(1-x)$PMN–xPT ceramic nanocomposites sintered at 1200 °C

sintering temperature on the phase formation, densification, microstructure, and electrical properties of the PMN–PT ceramic nanocomposites.

Acknowledgements This work was supported by the National Nanotechnology Center (NANOTEC), NSTDA, the Thailand Research Fund (TRF), the Commission on Higher Education (CHE) and the Faculty of Science, Chiang Mai University.

References

1. Ngamjarurojana A, Ananta S (2009) Chiang Mai J Sci 36:59
2. Tipakontitikul R, Ananta S, Yimnirun R (2006) Curr Appl Phys 6:307
3. Alexe M, Hesse D (2006) J Mater Sci 41:1. doi:10.1007/s10853-005-5912-x
4. Moulson AJ, Herbert JM (2003) Electroceramics, 2nd edn. Wiley, New York
5. Uchino K (2000) Ferroelectric devices. Marcel Dekker, New York
6. Haertling GH (1999) J Am Ceram Soc 82:797
7. Swartz SL, Shrout TR, Schulze WA, Cross LE (1984) J Am Ceram Soc 67:311
8. Guha JP, Hong DJ, Anderson HU (1988) J Am Ceram Soc 71:C-152
9. Wongmaneerung R, Sarakonsri T, Yimnirun R, Ananta S (2006) Mater Sci Eng B 130:246
10. Wongmaneerung R, Sarakonsri T, Yimnirun R, Ananta S (2006) Mater Sci Eng B 132:292
11. Koyuneu M, Pilgrim SM (1999) J Am Ceram Soc 82:3075
12. Kusumoto K, Sekiya T (1998) Mat Res Bull 33:1367
13. Niihara K (1991) J Ceram Soc Jpn 99:974
14. Kuntz JD, Zhan GD, Mukherjee AK (2004) MRS Bull 29:22
15. Hwang HJ, Nagai T, Sando M, Toriyama M, Niihara K (1999) J Eur Ceram Soc 19:993
16. Hwang HJ, Niihara K (1998) J Mater Sci 33:549. doi:10.1023/A:1004365006839
17. Tajima K, Hwang HJ, Sando M, Niihara K (1999) J Eur Ceram Soc 19:1179
18. Wongmaneerung R, Rujiwatra A, Yimnirun R, Ananta S (2008) J Alloys Compd 475:473
19. Chaisan W, Yimnirun R, Ananta S (2009) Ceram Int 35:121
20. Wongmaneerung R, Yimnirun R, Ananta S (2006) Mater Lett 60:1447
21. Wongmaneerung R, Yimnirun R, Ananta S (2006) Mater Lett 60:2666
22. Wongmaneerung R, Yimnirun R, Ananta S (2007) Appl Phys A 86:249
23. Fengbing S, Qiang L, Haisheng Z, Chunhong L, Shixi Z, Dezhong S (2004) Mater Chem Phys 83:135
24. Suh DH, Lee DH, Kim NK (2002) J Eur Ceram Soc 22:219
25. Wongsaenmai S, Tan X, Ananta S, Yimnirun R (2008) J Alloy Compd 454:331
26. Chaisan W, Yimnirun R, Ananta S, Cann DP (2006) Mat Sci Eng B 132:300
27. Ananta S, Thomas NW (1999) J Eur Ceram Soc 19:155
28. Gupta SM, Kulkarni AR (1994) Mater Chem Phys 39:98
29. Udomporn A, Pengpat K, Ananta S (2004) J Eur Ceram Soc 24:185
30. Ananta S, Thomas NW (1999) J Eur Ceram Soc 19:629
31. Ananta S, Thomas NW (1999) J Eur Ceram Soc 19:1873
32. Wang HC, Schulze WA (1990) J Am Ceram Soc 73:825
33. Choi SW, Jang JM, Bhalla AS (1996) Ferroelectrics 189:27
34. Kelly J, Leonard M, Tantigate C, Safari A (1997) J Am Ceram Soc 80:957
35. Wongmaneerung R, Yimnirun R, Ananta S (2009) Curr Appl Phys 9:268
36. Alguero M, Alemany C, Jimenez B, Holc J, Kosec M, Pardo L (2004) J Eur Ceram Soc 24:937
37. German RM (1996) Sintering theory and practice. Wiley, Chichester
38. Zhang J, Wang L, Shi L, Jiang W, Chen L (2007) Scripta Mater 56:241
39. Kong LB, Ma J, Zhu W, Tan OK (2002) Mat Res Bull 373:459
40. Cross LE (1987) Ferroelectrics 76:241
41. Unruan M, Wongmaneerung R, Ngamjarurojana A, Laosiritaworn Y, Ananta S, Yimnirun R (2005) J Appl Phys 104:064107
42. Unruan M, Ngamjarurojana A, Laosiritaworn Y, Ananta S, Yimnirun R (2005) J Appl Phys 104:034101
43. Yimnirun R, Ananta S, Laoratanakul P (2004) Mat Sci Eng B 112:79
44. Yimnirun R, Ananta S, Laoratanakul P (2005) J Eur Ceram Soc 25:3235
45. Koval V, Alemany C, Briancin J, Brunckove H (2003) J Electroceramics 10:19
46. Ausloo M (1985) J Phys C Solid State Phys 18:L1163
47. Wongsaenmai S, Laosiritaworn Y, Ananta S, Yimnirun R (2006) Mater Sci Eng B 128:83
48. Prasatkhetragarn A, Ketsuwan P, Ananta S, Yimnirun R, Cann DP (2009) Mater Lett 63:1281
49. Frey MH, Xu Z, Han P, Payne DA (1998) Ferroelectrics 206:337
50. Oh JH, Lee JH, Cho SH (1994) Ferroelectrics 158:241
51. Wongmaneerung R, Yimnirun R, Ananta S (2009) Mater Chem Phys 114:569